

Incorporation of charge transfer into the explicit polarization fragment method by grand canonical density functional theory

Miho Isegawa, Jiali Gao, and Donald G. Truhlar^{a)}

Department of Chemistry and Supercomputing Institute, University of Minnesota, Minneapolis, Minnesota 55455, USA

(Received 23 May 2011; accepted 11 July 2011; published online 23 August 2011)

Molecular fragmentation algorithms provide a powerful approach to extending electronic structure methods to very large systems. Here we present a method for including charge transfer between molecular fragments in the explicit polarization (X-Pol) fragment method for calculating potential energy surfaces. In the conventional X-Pol method, the total charge of each fragment is preserved, and charge transfer between fragments is not allowed. The description of charge transfer is made possible by treating each fragment as an open system with respect to the number of electrons. To achieve this, we applied Mermin's finite temperature method to the X-Pol wave function. In the application of this method to X-Pol, the fragments are open systems that partially equilibrate their number of electrons through a quasithermodynamics electron reservoir. The number of electrons in a given fragment can take a fractional value, and the electrons of each fragment obey the Fermi–Dirac distribution. The equilibrium state for the electrons is determined by electronegativity equalization with conservation of the total number of electrons. The amount of charge transfer is controlled by re-interpreting the temperature parameter in the Fermi–Dirac distribution function as a coupling strength parameter. We determined this coupling parameter so as to reproduce the charge transfer energy obtained by block localized energy decomposition analysis. We apply the new method to ten systems, and we show that it can yield reasonable approximations to potential energy profiles, to charge transfer stabilization energies, and to the direction and amount of charge transferred. © 2011 American Institute of Physics. [doi:10.1063/1.3624890]

I. INTRODUCTION

Charge transfer interaction was introduced into theoretical chemistry by Mulliken and others^{1,2} to explain the attractive interaction in complexes that could not be classified according to the interaction types previously recognized, in particular, ionic, covalent, and hydrogen bonds. Since then, charge transfer systems have been extensively studied by experiment, calculations, and model development.^{3–6} We are concerned here with charge transfer between interacting molecules or fragments in their ground electronic states, and from the point of view of molecular orbital theory, such charge transfer is recognized as the migration of electron density primarily from the highest occupied molecular orbital (HOMO) of an electron donor to the lowest unoccupied molecular orbital (LUMO) of an electron acceptor. Charge transfer is included in molecular modeling by treating the complex as a supermolecule, and, if desired, the specific contribution of charge transfer to the complex's energy can be identified by energy decomposition methods.^{7–10} The application of decomposition methods to a wide range of systems has made clear the role of the charge transfer interaction in both simple and complex systems.^{11–15}

Electron transfer is important not just in charge transfer complexes^{1,2} (where it provides the dominant contribution to binding) but to some extent in all interatomic and

intermolecular interactions, except for high-symmetry cases in small systems. Neglect of charge transfer interactions in molecular modeling has the consequence that the electron densities and/or charge distributions upon which the modeling is based have systematic errors. In recent years, considerable attention has been devoted to including polarization in molecular modeling methods,^{16–28} but usually without including charge transfer between interacting molecules or molecular fragments. This is unbalanced because charge transfer is actually an extreme form of polarization, where the polarized charge moves a significant distance and cannot be well approximated as a linear response.

The explicit polarization (X-Pol) method^{29–32} is a model that describes polarization by a quantum mechanical treatment of molecular electron densities (as opposed to many other models that are essentially classical, such as molecular mechanics). In this model, a condensed-phase system is divided into interacting fragments, the internal energies of the fragments are treated with quantum mechanical electronic structure theory, and the interactions between fragments are described by electrostatics and empirical functions for the description of exchange repulsion and dispersion-like interactions between fragments. The sum of these exchange repulsion and dispersion-like interactions is called the van der Waals energy. The true interfragment interaction may be decomposed into five components: electrostatic, polarization, exchange-repulsion, dispersion, and charge transfer interactions. In the X-Pol method, the electrostatic interaction can be

^{a)}Electronic mail: truhlar@umn.edu.

described using a variety of approaches, including the approximation used here that the electrostatic potential of the other fragments is given by the Coulomb potential of partial atomic charges^{29,31,32} (one can also use multipole moments³³). The exchange repulsion interactions can be estimated by antisymmetrizing the X-Pol wave function³⁴ using the block-localized wave function (BLW) approach.¹⁰ The exchange repulsion is short-ranged and approximately pairwise additive, and so here and in most previous work we approximate it by the short range term of Lennard-Jones potentials. Dispersion is also included by Lennard-Jones potentials, and the polarization is included by a self-consistent field quantum mechanical model. Charge transfer interaction between fragments that are not connected by a covalent bond is not included in the original X-Pol method because the fragments each have a fixed number of electrons.

The requirement that fragments have a fixed integer number of electrons presents a barrier to including charge transfer in all quantum mechanical fragment models. Li *et al.*³⁵ included the charge transfer interaction in the framework of the effective fragment method^{36,37} based on the second-order perturbation method. In the perturbation method, the stabilization energy by the charge transfer is included by the combination of occupied molecular orbitals of one fragment with the virtual molecular orbitals of another fragment. The perturbation method was also used in the study by Stone.³⁸ However, the perturbation approach lacks self-consistency steps and behaves correctly only when the interaction is relatively small.

In this work, we construct a self-consistent fragment-based charge transfer model that predicts the direction and amount of charge transfer from one fragment to the other fragment and provides an estimate of the stabilization energy due to charge transfer. The method is an extension of X-Pol, and we call it grand canonical-X-Pol or GC-X-Pol. It is applicable to both weak van der Waals interactions and to the fairly strong interactions in systems that include charged species. In order to describe the migration of electrons from one fragment to another, one needs to treat each fragment as an open system with respect to the number of electrons. Mermin's finite temperature method³⁹ makes this possible, because the electrons in a molecule are treated with the grand canonical ensemble and the electron distribution is determined by Fermi-Dirac⁴⁰ statistics. Mermin's theory is an extension of the Hohenberg-Kohn theorem⁴¹ and reduces to conventional density functional theory in the case of zero temperature. It has been applied to electrochemical processes⁴² and to the dynamics of quantum fluids.⁴³⁻⁴⁶ In our application of this theory to the X-Pol fragment method, the distribution of electrons between fragments is determined based on the concept of chemical potential equalization, which is also called electronegativity equalization. This concept was originally suggested by Sanderson⁴⁷ and has been rigorously defined in density functional theory.^{48,49} A large number of applications have proved that this concept is a useful tool to determine the redistribution of charge densities during chemical processes.⁵⁰⁻⁶⁶ Much of the previous work on electronegativity equilibration algorithms has been in the context of polarizable molecular mechanics and semiempirical valence bond theory, but we note that the method has also previously been applied⁶⁷ in a quan-

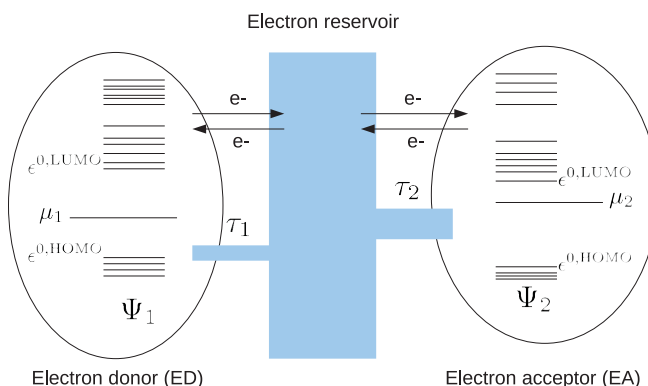


FIG. 1. Electron donor (ED) and acceptor (EA) combined via an electron reservoir with coupling strength τ_1 and τ_2 , respectively. $\epsilon^{0,\text{HOMO}}$ and $\epsilon^{0,\text{LUMO}}$ are labeled for the orbitals of the HOMO and the LUMO at zero coupling. μ_1 and μ_2 are chemical potentials and these are located on between the HOMO and the LUMO. The right and left arrows indicate that the system is in an equilibrium state for the electrons.

tum mechanical fragment method, which is the subject of the present paper.⁶⁷

II. METHOD

II.A. Mermin's free-energy functional in X-Pol

We consider a system which is composed of N_f fragments. For example, each fragment can be a molecule or ion in a liquid system or a residue in a protein. Each fragment is coupled to the others via an electron reservoir as shown in Fig. 1, and the fragments exchange electrons through the reservoir. The grand canonical energy for a fragment α is given by³⁹

$$F_\alpha[\rho_\alpha(\mathbf{r})] = T_\alpha[\rho_\alpha(\mathbf{r})] + J_\alpha[\rho_\alpha(\mathbf{r})] + \Omega_{\text{xc},\alpha}[\rho_\alpha(\mathbf{r})] - \theta S_\alpha[\rho_\alpha(\mathbf{r})] + \int (v_{\text{ext}}(\mathbf{r}) - \mu) \rho_\alpha(\mathbf{r}) d\mathbf{r} + E_\alpha^{\text{nuc}}, \quad (1)$$

where the first term is the electronic kinetic energy, and the second and third terms are electron-electron Coulomb energy and exchange-correlation energy, respectively. The first and second energy terms are given by

$$T_\alpha[\rho_\alpha(\mathbf{r})] = \sum_i^{M_\alpha} f_{\alpha,i} \int \psi_{\alpha,i}(\mathbf{r}) \left(-\frac{\nabla^2}{2} \right) \psi_{\alpha,i}(\mathbf{r}) d\mathbf{r} \quad (2)$$

and

$$J_\alpha[\rho_\alpha(\mathbf{r})] = \frac{1}{2} \iint \frac{\rho_\alpha(\mathbf{r}) \rho_\alpha(\mathbf{r}')}{|\mathbf{r} - \mathbf{r}'|} d\mathbf{r} d\mathbf{r}', \quad (3)$$

where $\psi_{\alpha,i}(\mathbf{r})$ is the i th molecular orbital and M_α is the number of orbitals in fragment α . Note that in closed-shell fragments the up-spin and down-spin spatial orbitals are identical, in which case each spatial orbital occurs twice. In Eq. (2), $f_{\alpha,i}(\epsilon_{\alpha,i})$ is orbital occupancy which is represented by the Fermi-Dirac distribution function,

$$f_{\alpha,i}(\epsilon_{\alpha,i}) = \frac{1}{1 + \exp\left(\frac{\epsilon_{\alpha,i} - \mu}{k_B \theta}\right)}. \quad (4)$$

Here $\epsilon_{\alpha,i}$ is the orbital energy of the i th molecular orbital, μ is the chemical potential that characterizes the whole system, and k_B and θ are the Boltzmann constant and the temperature, respectively.

At zero temperature, μ is equal to the Fermi energy ϵ_F , and the occupancy function becomes a Heaviside function,

$$f_{\alpha,i}(\epsilon_{\alpha,i}) = \begin{cases} 1 & (\epsilon_{\alpha,i} < \epsilon_F) \\ 0 & (\epsilon_{\alpha,i} > \epsilon_F). \end{cases} \quad (5)$$

The orbitals that have zero occupancy in this limit are called virtual orbitals.

The fourth term in Eq. (1) is the contribution of the entropy, where the entropy for Fermi particles is given by

$$S_{\alpha}[\rho_{\alpha}(\mathbf{r})] = -k_B \sum_i^{M_{\alpha}} \{f_{\alpha,i} \ln f_{\alpha,i} + (1 - f_{\alpha,i}) \ln(1 - f_{\alpha,i})\}. \quad (6)$$

The entropy term has a nonzero value only when one or more of the orbitals is occupied by a fractional number of electrons.

In the fifth term in Eq. (1), $v_{\text{ext}}(\mathbf{r})$ is the potential from sources external to the electronic subsystem of fragment α ; this includes the interaction of the electrons in fragment α with the nuclei of fragment α and with the electrostatic field due to the other fragments. Therefore, the interaction between the external potential and the electron density in fragment α is given by

$$\int v_{\text{ext}}(\mathbf{r})\rho_{\alpha}(\mathbf{r})d\mathbf{r} = -\sum_{a \in \alpha}^{N_{\alpha}} \int \frac{Z_a}{|\mathbf{r} - \mathbf{R}_a|} \rho_{\alpha}(\mathbf{r})d\mathbf{r} - \sum_{\beta \neq \alpha}^{N_f} \sum_{b \in \beta}^{N_{\beta}} \int \frac{q_b}{|\mathbf{r} - \mathbf{R}_b|} \rho_{\alpha}(\mathbf{r})d\mathbf{r}, \quad (7)$$

where N_{α} and N_f are the number of atoms in fragment α and the number of fragments, respectively, and \mathbf{R}_a is the coordinate of nucleus a . The terms in Eq. (7) represent interactions of electrons with the nuclear charges $\{Z_{\alpha}\}$ in the same fragment α and with the partial atomic charges $\{q_b\}$ in the remaining fragments. The chemical potential also affects the motion of electrons, such that the electrons move in the effective potential $v_{\text{ext}} - \mu_{\alpha}$. The last term in Eq. (1) represents nuclear-nuclear repulsion interaction energies.

At a finite temperature, the equilibrium system is assumed to be a mixture of ground and excited states, and we observe some electron density in the virtual orbitals. The electron density in fragment α is expressed as

$$\rho_{\alpha}(\mathbf{r}) = \sum_{i=1}^{M_{\alpha}} f_{\alpha,i}(\epsilon_{\alpha,i}) |\psi_{\alpha,i}(\mathbf{r})|^2. \quad (8)$$

The number of electrons in each fragment is not fixed because each fragment can exchange electrons with other fragments via the electron reservoir; however, the total number of electrons in the whole system, N_{tot} , is preserved as

$$\sum_{\alpha} \sum_{i \in \alpha}^{M_{\alpha}} f_{\alpha,i} = N_{\text{tot}}. \quad (9)$$

The actual charge transfer interactions in the systems we study are not caused by a finite temperature; however, we use the finite-temperature ensemble with an artificially raised temperature to model the correction to the approximation that each fragment has a fixed number of electrons. The determination of the temperature parameter is explained in Section IV.

The molecular orbitals that minimize the grand canonical potential energy are obtained by solving the grand canonical Kohn–Sham (KS) equations at a finite temperature θ and chemical potential μ ,

$$\left\{ -\frac{\nabla^2}{2} - \sum_{a \in \alpha}^{N_{\alpha}} \frac{Z_a}{|\mathbf{r} - \mathbf{R}_a|} + \int \frac{\rho_{\alpha}(\mathbf{r}')}{|\mathbf{r} - \mathbf{r}'|} d\mathbf{r}' + \sum_{\beta \neq \alpha}^{N_f} \sum_{b \in \beta}^{N_{\beta}} \frac{q_b}{|\mathbf{r} - \mathbf{R}_b|} + w_{\text{xc},\alpha,i}(\mathbf{r}) \right\} \psi_{\alpha,i}(\mathbf{r}) = \epsilon_{\alpha,i} \psi_{\alpha,i}(\mathbf{r}), \quad (10)$$

where $w_{\text{xc},\alpha,i}(\mathbf{r})$ is exchange-correlation potential defined by

$$w_{\text{xc},\alpha,i}(\mathbf{r}) \equiv \frac{\delta E_{\text{XC}}}{\delta \rho_{\alpha,i}(\mathbf{r})}. \quad (11)$$

Equation (10) differs from the conventional zero-temperature KS equation in that the electron density is represented with fractional occupation numbers. The grand canonical Kohn–Sham operator is the operator in the braces of Eq. (10). It depends implicitly on μ because it involves the electron density, which depends on the chemical potential through Eqs. (4) and (8).

Using the molecular orbitals obtained from Eq. (10), one can calculate the grand canonical energy of fragment α from a formula analogous to that used in Hartree–Fock (HF) theory,

$$F_{\alpha} = E_{\alpha} - \theta S_{\alpha} - N_{\alpha} \mu_{\alpha} = \frac{1}{2} \sum_{\lambda}^{M_{\alpha}} \sum_{\nu}^{M_{\alpha}} \tilde{P}_{\alpha,\lambda\nu} (H_{\alpha,\lambda\nu}^{\text{core}} + F_{\alpha,\lambda\nu}) - \theta S_{\alpha} - N_{\alpha} \mu_{\alpha}. \quad (12)$$

In Eq. (12), $F_{\alpha,\lambda\nu}$ is an element of the Fock matrix, and $H_{\alpha,\lambda\nu}^{\text{core}}$ is defined as⁶⁹

$$H_{\alpha,\lambda\nu}^{\text{core}} = \int \phi_{\alpha,\lambda}^* \left[-\frac{1}{2} \nabla^2 - \sum_{a \in \alpha}^{N_{\alpha}} \frac{Z_a}{|\mathbf{r} - \mathbf{R}_a|} - \sum_{\beta \neq \alpha}^{N_f} \sum_{b \in \beta}^{N_{\beta}} \int \frac{q_b}{|\mathbf{r} - \mathbf{R}_b|} \right] \phi_{\alpha,\nu} d\mathbf{r}, \quad (13)$$

where the indices λ and ν refer to the atomic orbitals, and $\tilde{P}_{\alpha,\lambda\nu}$ is a density matrix element that can be written using fractional occupancies as

$$\tilde{P}_{\alpha,\lambda\nu} = \sum_i^{M_{\alpha}} f_{\alpha,i} c_{\alpha,\lambda i} c_{\alpha,\nu i}, \quad (14)$$

where $c_{\alpha,\lambda i}$ is the coefficient of the λ th atomic orbital in molecular orbital i of fragment α .

Then the total energy of the entire system is written as

$$E^{\text{X-Pol}} = \sum_{\alpha}^{N_f} U_{\alpha} + \frac{1}{2} \sum_{\alpha}^{N_f} \sum_{a \in \alpha}^{N_{\alpha}} \sum_{\beta \neq \alpha}^{N_f} \sum_{b \in \beta}^{N_{\beta}} \frac{q_b Z_a}{|\mathbf{R}_b - \mathbf{R}_a|} + E^{\text{vdw}}, \quad (15)$$

where

$$U_{\alpha} = E_{\alpha} - \theta S_{\alpha}. \quad (16)$$

Note that Eq. (15) excludes the chemical potential contribution of the grand canonical energy F_{α} . Because S_{α} is very small, U_{α} is almost equal to the electronic energy E_{α} , which is as a sum of the kinetic and potential energies of the electron. The second and third term in Eq. (15) represent the Coulomb and van der Waals interactions between fragments, respectively. In the present study, the partial charge is determined by Mulliken population analysis,⁷⁰ and the Mulliken charge is given by

$$q_b = Z_b - \sum_{\mu \in b}^{M_{\beta}} (\tilde{\mathbf{P}}\mathbf{S})_{\mu}, \quad (17)$$

where \mathbf{S} is the overlap integral. The van der Waals interactions are determined using the Lennard-Jones potential function,

$$E^{\text{vdw}} = \sum_a^{N_{\alpha}} \sum_b^{N_{\beta}} 4\epsilon_{ab} \left[\left(\frac{\sigma_{ab}}{R_{ab}} \right)^{12} - \left(\frac{\sigma_{ab}}{R_{ab}} \right)^6 \right]. \quad (18)$$

The pairwise parameters ϵ_{ab} and σ_{ab} are derived from atomic parameters ϵ_a , ϵ_b , σ_a , and σ_b by using combining rules:

$$\epsilon_{ab} = \sqrt{\epsilon_a \epsilon_b} \quad (19a)$$

$$\sigma_{ab} = \frac{\sigma_a + \sigma_b}{2} \quad (19b)$$

Notice that hardness is included automatically in the present model by the full electronic structure calculation on each fragment.

II.B. Fermi–Dirac distribution function for X-Pol

According to the electronegativity equalization principle, the chemical potential is the same in every fragment of the complex. However, in a fragment method, we are not treating true thermodynamic equilibrium, and the degree of equalization should depend on the strength of coupling between a pair of fragments, and this coupling strength is a function of the distance between them. For example, when the two fragments are infinitely separated, the chemical potential of each fragment is independent of the other fragment because the

two fragments are no longer coupled to a common electron reservoir. The need for introducing partial equilibration when overlap is diminished is well established in the literature of electronegativity equilibration.^{58,59,61,62,64,68} If a fragment is infinitely separated from all other fragments, then its chemical potential is the same as that in the gas phase, and as two fragments approach, the coupling becomes significant, and each fragment is characterized by the same chemical potential (we call the common chemical potential the universal chemical potential). We include this distance effect by writing,

$$\mu_{\alpha} = g_{\alpha} \tilde{\mu} + (1 - g_{\alpha}) \mu_{\alpha}^0(\tau_{\alpha}), \quad (20)$$

where $\mu_{\alpha}^0(\tau_{\alpha})$ is the chemical potential of the constituent fragment that combines with the electron reservoir with coupling strength τ_{α} , $\tilde{\mu}$ is the universal chemical potential for the entire system based on the self-consistent equations for the coupled fragments, and g_{α} is the weight of the universal chemical potential $\tilde{\mu}$ as specified below.

The Fermi–Dirac distribution depends on both the temperature and the chemical potential. In the Fermi–Dirac distribution function, the occupancies of the virtual orbitals increase with increasing temperature, and this controls the amount of charge transfer. In order to reflect the dependency of the coupling strength on the interfragment distance, we rewrite the Fermi–Dirac distribution function as

$$f_{\alpha,i} = \frac{1}{1 + \exp\left(\frac{\epsilon_{\alpha,i} - \mu_{\alpha}}{\tau_{\alpha}}\right)} \quad (21)$$

where τ_{α} is coupling strength defined by

$$\tau_{\alpha} \equiv k_B \theta g_{\alpha}. \quad (22)$$

The weight g_{α} is an exponentially decaying pairwise function of the effective distance between atomic sites, and it determines the balance between the universal chemical potential and the chemical potential of the single fragment α . At infinite separation of a given fragment from all other fragments, g_{α} becomes zero, and the coupling strength becomes zero. The weight takes a value between 0 and 1 and is given by

$$g_{\alpha}(\tilde{R}_{ab}) = \frac{1}{N_{\beta}} \sum_{b \in \beta}^{N_{\beta}} \frac{1}{N_{\alpha}} \sum_{a \in \alpha}^{N_{\alpha}} e^{-\zeta \tilde{R}_{ab}}, \quad (23)$$

where N_{α} and N_{β} are the numbers of atoms in fragments α and β , respectively, and ζ is a constant parameter that determines the dependence on the effective distance \tilde{R}_{ab} between atom a in fragment α and atom b in fragment β . The effective distance is given by

$$\tilde{R}_{ab} = \begin{cases} 0, & (R_{ab} < \tilde{\sigma}_{ab}) \\ S_{\text{pl}}(R_{ab}) = \alpha(R_{ab} - \tilde{\sigma}_{ab})^3 + \beta(R_{ab} - \tilde{\sigma}_{ab})^4 + \gamma(R_{ab} - \tilde{\sigma}_{ab})^5, & (\tilde{\sigma}_{ab} \leq R_{ab} \leq \tilde{\sigma}_{ab} + \Delta) \\ R_{ab}, & (R_{ab} > \tilde{\sigma}_{ab} + \Delta) \end{cases} \quad (24)$$

where the two functions $\tilde{R}_{ab} = 0$ and $\tilde{R}_{ab} = R_{ab}$ are smoothly connected by the spline function $S_{\text{pl}}(\tilde{R}_{ab})$ in the region between $\tilde{\sigma}_{ab}$ and $\tilde{\sigma}_{ab} + \Delta$. The coefficients of the spline function are given by

$$\alpha = \frac{10}{\Delta^3} (\Delta + \tilde{\sigma}_{ab}) - \frac{4}{\Delta^2}, \quad (25)$$

$$\beta = \frac{-15}{\Delta^4} (\Delta + \tilde{\sigma}_{ab}) + \frac{7}{\Delta^3}, \quad (26)$$

$$\gamma = \frac{6}{\Delta^5} (\Delta + \tilde{\sigma}_{ab}) - \frac{3}{\Delta^4}. \quad (27)$$

These are obtained by solving the linear equations yielded by imposing three continuity conditions for the function and its first two derivatives at each boundary. The pairwise parameter $\tilde{\sigma}_{ab}$ is written as

$$\tilde{\sigma}_{ab} = \kappa (\tilde{\sigma}_a + \tilde{\sigma}_b), \quad (28)$$

where $\tilde{\sigma}_a$ is the van der Waals radii of atom a . In Eqs. (24)–(27), Δ and κ are constant parameters which are independent of the type of atom or the system. Because Eq. (23), like overlap, decreases exponentially with distance, its use should eliminate the superlinear scaling and unphysical polarizabilities encountered^{59,63,64} in early versions of electronegativity equalization based on molecular mechanics. The use of Eq. (23) also avoids the problem of dissociation to ion instead of neutral fragments.⁶⁰

III. COMPUTATIONAL DETAILS

In the conventional X-Pol method, double self-consistent field (SCF) optimizations are performed.^{29,31,32} One of the SCF procedures corresponds to molecular orbital optimizations for the individual fragments under the external electrostatic potential of the remaining fragments. In the nonvariational version of X-Pol that is used here, this electrostatic potential is the same as is used in quantum mechanical/molecular mechanical (QM/MM) calculations based on partial atomic charges. The other SCF calculation is performed to obtain the full relaxation of the electronic polarization over the entire system. In this procedure, the wave function of given fragments and the charges of the remaining fragments are alternately (or simultaneously) updated. The double SCF calculations are continued until the total energy of the whole system converges. In addition to the above SCF calculations, one more iterative calculation is required in the GC-X-Pol method in order to determine a universal chemical potential that characterizes the system. The procedure including the triple SCF calculations is illustrated with the flowchart in Fig. 2. The initial chemical potential of a fragment α that is coupled to the electron reservoir is given by

$$\mu_{\alpha}^{0,\text{init}} = \frac{\epsilon_{\alpha}^{\text{HOMO}}(0) + \epsilon_{\alpha}^{\text{LUMO}}(0)}{2}, \quad (29)$$

where superscript “0” indicates the isolated fragment, and $\epsilon_{\alpha}^{\text{HOMO}}(0)$ and $\epsilon_{\alpha}^{\text{LUMO}}(0)$ are respectively orbital energies of the HOMO and LUMO at zero temperature. This equation

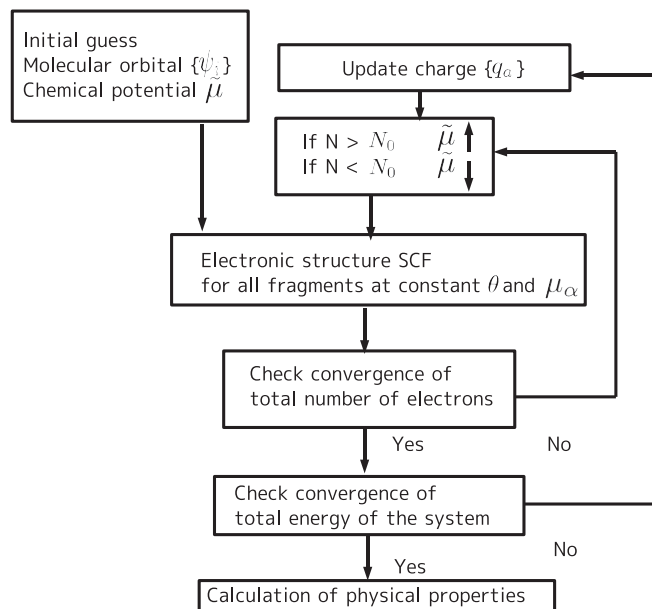


FIG. 2. Flowchart of triple SCF procedures in GC-X-Pol method.

originates from Mulliken’s definition of absolute electronegativity,

$$\chi = \frac{IP + EA}{2}, \quad (30)$$

where IP and EA are the ionization potential and electron affinity, respectively. For this purpose, the IP and EA are approximated by orbital energies:

$$IP \approx \epsilon_{\alpha}^{\text{HOMO}}(0) \quad (31a)$$

and

$$EA \approx \epsilon_{\alpha}^{\text{LUMO}}(0), \quad (31b)$$

where Eq. (31a) is Koopmans’s theorem.⁷¹ The initial universal chemical potential is given as an average of the chemical potentials of constituent single fragments,

$$\tilde{\mu}^{\text{init}} = \sum_{\alpha} \mu_{\alpha}^0(\tau_{\alpha}) / N_f. \quad (32)$$

At each iteration, the electronic structure of each fragment is determined under the constant chemical potential μ_{α} and coupling strength τ_{α} , where the occupancies change in each iteration step of the SCF procedure because the occupancies are functions of the molecular orbital energies. After the molecular orbitals are optimized for the all of fragments, the number of electrons in the whole system is checked. The chemical potential is increased when the total number of electrons is smaller than the original number of electrons and is reduced when the number is exceeded. This adjustment is continued until the total number of electrons in the entire system reaches the original integer number. To achieve smooth convergence of the chemical potential, we used the following function for the adjustments:

$$\Delta\mu_j = E_h C \Delta N_j \quad (33)$$

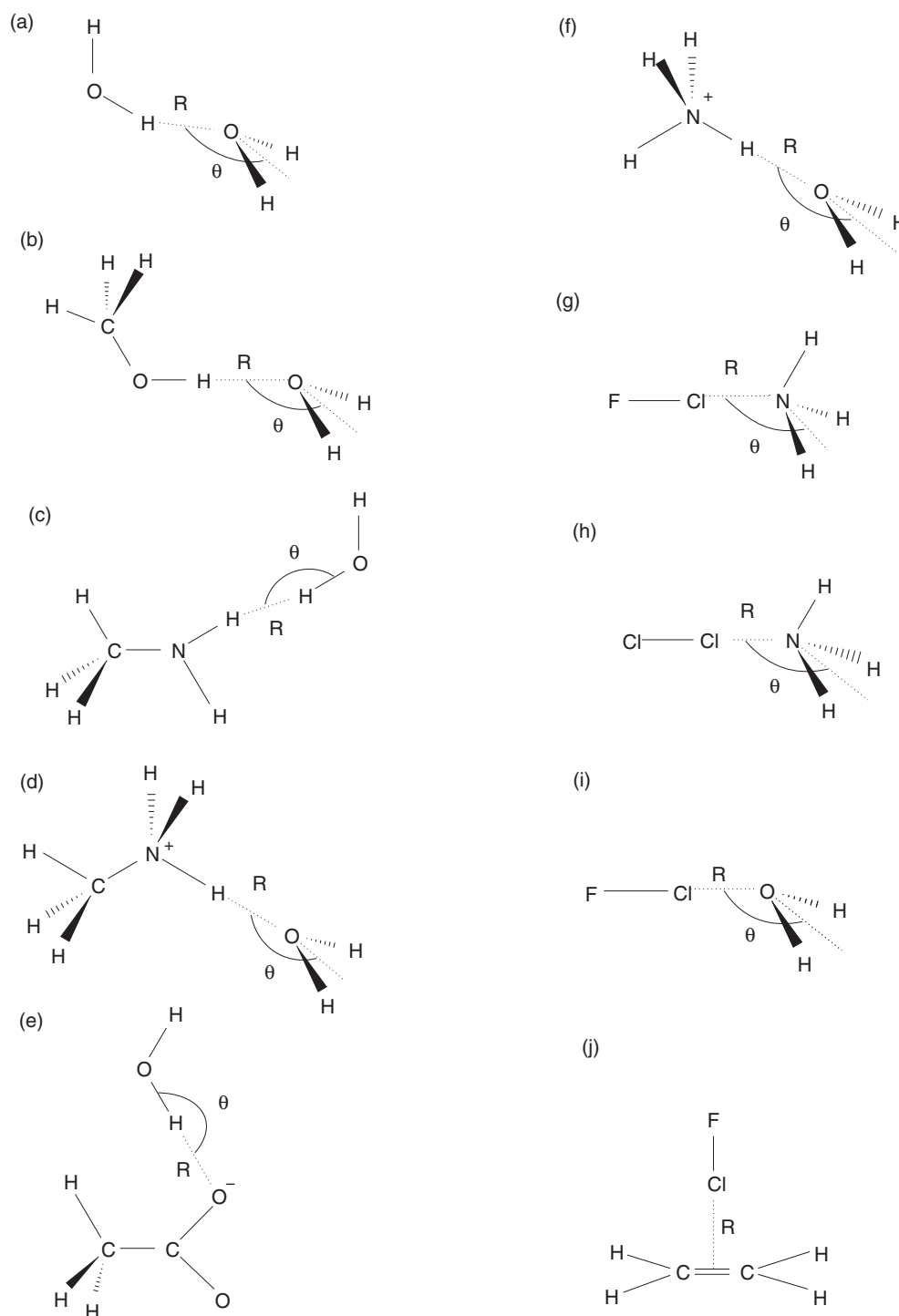


FIG. 3. Chemical structures of ten dimer systems with the definitions of R and θ . (a)–(c) are hydrogen bonded systems of neutral dipole-dipole complexes, (d)–(f) are hydrogen bonded systems of ion-dipole pairs, (g)–(j) are charge transfer systems.

with

$$\Delta N_j = N_j - N_0, \quad (34)$$

where E_h is one hartree, C is unitless, and ΔN_j is the difference of the number of electrons at the j th iteration step N_j and the original number of electrons N_0 . Note that Eq. (33) is obtained by a first-order truncation of the Fermi-Dirac distribution. The initial value of C is 1.0 and the value is changed in each SCF iteration step as following. When the

number of electrons fluctuates around the original number of electrons, we multiply C by a factor $0.0 < C_{\text{fluctuation}} < 1.0$. On the other hand, when the number of electrons is continuously under or over of the original number of electrons, we multiply C by $1.0 < C_{\text{monotonic}} < 2.0$. Thus, C is written as a product of powers of $C_{\text{fluctuation}}$ and $C_{\text{monotonic}}$. The threshold for each SCF procedure is 10^{-7} electron for the total number of electrons, 10^{-6} hartrees for the electronic energy of each fragment, and 10^{-7} hartrees for the X-Pol energy of the

TABLE I. Optimized intermolecular distance R [Å] and angle θ [degree].

	R^a	θ^b
(a) H ₂ O...H ₂ O	1.92	140.7
(b) CH ₃ OH...H ₂ O	1.92	139.5
(c) CH ₃ NH ₂ ...H ₂ O	2.15	135.5
(d) CH ₃ NH ₃ ⁺ ...H ₂ O	1.71	180.0 ^b
(e) CH ₃ CO ₂ ⁻ ...H ₂ O	1.69	122.5
(f) NH ₄ ⁺ ...H ₂ O	1.68	180.0 ^b
(g) ClF...NH ₃	2.43	127.0
(h) Cl ₂ ...NH ₃	2.64	126.3
(i) ClF...H ₂ O	2.55	134.7
(j) ClF...C ₂ H ₄	2.83	...

^aThe definitions of R and θ are given in Fig. 3.

^bThe value is fixed to avoid the flip of the water molecule at large R and to define a reaction coordinate that yields a smooth binding energy profile.

entire system. The actual number of interactions required to achieve convergence will depend on the algorithm used. The algorithm presented above is a straightforward one but it's not optimized. Optimization of the iteration scheme is subject for future study.

All of the geometries are optimized using the M06-2X density functional⁷² with the 6-31+G(d,p) (Ref. 73) basis set. The dimer geometries are determined by partial optimization with the internal geometry of each monomer fixed. The optimized intermolecular coordinates are summarized in Table I. In the X-Pol calculation for both 0 K and finite temperature, the energies are calculated using M06-2X with the 6-31G(d) (Ref. 73) basis set because this basis set provides reasonable Mulliken charge distributions.³² (However, one can also use more accurate charge models⁷⁴⁻⁷⁶ in future work.) In the numerical calculation of the exchange-correlation energy, polar coordinates are employed for the grid generation. The number of grid points is as follows. Ninety-six radial points in the Euler-MacLaurin quadrature, 20 points for angle theta, and 40 points for angle phi grids in the Gauss-Legendre quadrature. This number of grid points provides enough accuracy for the comparison of eigenvalues between different conformers for the identical molecule.

Lennard-Jones (LJ) parameters are important for the accurate estimate of interaction energy between QM and MM fragments.^{77,78} The present LJ parameters are taken from the previous X-Pol work³² for C, O, and N atoms except that here we use an arithmetic mean in Eq. (19b), and Ref. 32 used a geometric mean. These parameters were optimized for the B3LYP/6-31G(d) model so as to reproduce the equilibrium geometries and the binding energies determined by electronic structure calculations (therefore, these parameters need not be the optimal ones for the present M06-2X functional, but they will suffice to illustrate the new method). For the O atom, we took the average value for those of the sp² and sp³ hybridization states. The parameters of F and Cl are the same as those used in the generalized AMBER force field,⁷⁹ except for epsilon of Cl. Both ϵ_H and σ_H are parametrized in the present study so as to yield reasonable binding energy surfaces for hydrogen bonded systems, and σ_{Cl} is parametrized for the reference charge transfer systems. The LJ parameters that we used are summarized in Table II.

TABLE II. Lennard-Jones parameters.

	H ^a	C ^b	N ^b	O	F ^d	Cl
σ [Å]	1.100	3.650	3.450	3.225 ^c	3.120	2.610 ^a
ϵ [kcal/mol]	0.080	0.150	0.200	0.150 ^b	0.061	0.265 ^d

^aDetermined in the present study.

^bTaken from Ref. 32.

^cTaken average for two hybridization states, sp² and sp³ in Ref. 32.

^dTaken from Ref. 79.

IV. PARAMETRIZATION

Mermin's grand canonical method is incorporated in the X-Pol method in Subsection II A, and in Subsection II B we included the distance effect using weight function g_α in the Fermi-Dirac distribution function in order to take account of the vanishing of the coupling when the subsystems are separated. In the weight function g_α , three kind of parameters, ζ , Δ , and van der Waals radii, are included. We used Bondi's values⁸⁰ for the atomic radii: $\tilde{\sigma}_H = 1.20$, $\tilde{\sigma}_O = 1.52$, $\tilde{\sigma}_C = 1.70$, $\tilde{\sigma}_N = 1.55$, $\tilde{\sigma}_F = 1.47$, $\tilde{\sigma}_{Cl} = 1.75$ in Å. Thus, the present charge transfer model has three parameters still to be determined: ζ , Δ , and temperature θ . The absolute coupling strength is determined by θ , and ζ and Δ have less of an effect on the main results. Therefore, we parametrize θ for reasonable values of ζ and Δ . In the present, we set $\zeta = 0.05 a_0^{-1}$ and $\Delta = 1.0$ Å.

The parametrization of θ is carried out so as to reproduce the charge transfer energy yielded by the BLW energy decomposition method (BLW-ED).¹⁰ Figure 2 shows ten dimer systems used for the parametrization; these include 6 hydrogen bonded systems and 4 charge transfer systems.^{6,81-83}

In GC-X-Pol, the charge transfer interaction energy is defined by

$$\Delta E_{AB}^{CT,GC-X-Pol} \equiv \Delta E_{AB}^{GC-X-Pol}(\tau_\alpha, \tau_\beta) - \Delta E_{AB}^{X-Pol}(0), \quad (35)$$

where $\Delta E_{AB}^{GC-X-Pol}(\tau_\alpha, \tau_\beta)$ is the GC-X-Pol binding energy calculated by

$$\Delta E_{AB}^{GC-X-Pol}(\tau_\alpha, \tau_\beta) = E_{AB}^{GC-X-Pol}(\tau_\alpha, \tau_\beta) - E_A^{GC-X-Pol}(\tau_\alpha) - E_B^{GC-X-Pol}(\tau_\beta), \quad (36)$$

and where $\Delta E_{AB}^{X-Pol}(0)$ is the binding energy calculated by X-Pol without charge transfer, which is given by setting θ equal to zero:

$$\Delta E_{AB}^{X-Pol}(0) = E_{AB}^{X-Pol}(0) - E_A(0) - E_B(0), \quad (37)$$

where $E_{AB}^{X-Pol}(0)$ is the conventional X-Pol energy, and $E_A(0)$ is the monomer energy at zero temperature. Note that in Eq. (36), the reference state is defined as the isolated fragments each coupled to the electron reservoir with the same coupling strength that they have in the dimer. This definition is necessary to treat the kinetic energy of the electrons consistently in the coupled and uncoupled states. Note that the charge transfer energy in Eq. (36) may be considered as a model to mimic the electron delocalization effect as defined in the BLW Ref. 10 decomposition scheme, and the procedure should not be interpreted as yielding a physical wave function; that is important because the charge transfer energy

is not the difference between the GC energy and the energy of X-Pol, but rather it is an addition to the X-Pol energy based on the difference of terms calculated with nonzero coupling strengths, whereas the X-Pol wave function has zero coupling strength.

The quantity that is minimized in the parameter optimization is the root-mean square (RMS) deviation of the charge transfer energy predicted by GC-X-Pol from that predicted by the BLW-ED method; this is given by

$$R(\theta) = \sqrt{\frac{1}{N_s} \sum_{I_s}^{N_s} (\Delta E_{I_s}^{\text{CT,GC-X-Pol}}(\theta) - \Delta E_{I_s}^{\text{CT,BLW}})^2}, \quad (38)$$

where N_s is the total number of test systems. In the BLW method, the charge transfer energy is defined as

$$\Delta E^{\text{CT,BLW}} = E(\Psi_{\text{AB}}) - E(\Psi_{\text{AB}}^{\text{BLW}}), \quad (39)$$

where Ψ_{AB} is the fully optimized wave function for dimer AB, and $\Psi_{\text{AB}}^{\text{BLW}}$ is a block localized wave function defined by

$$\Psi_{\text{AB}}^{\text{BLW}} = \hat{A} \{ \Psi_{\text{A}} \Psi_{\text{B}} \}, \quad (40)$$

where Ψ_{A} represents a wave function that includes the polarization (intramolecular charge redistribution) and exchange interactions, and \hat{A} is an antisymmetrizer. It is noted that the migration of electrons between fragments A and B (intermolecular charge redistribution) is not allowed in the wave function $\Psi_{\text{AB}}^{\text{BLW}}$. In order to allow charge transfer, it is required to expand the orbitals of each monomer to the space of the entire system. Thus, BLW and X-Pol have the same definition of charge transfer from the point of view that the all of interactions except for charge transfer are based on the localized wave function in each fragment, although BLW also includes exchange repulsion explicitly.

V. RESULTS AND DISCUSSION

V.A. Effect of coupling strength on charge transfer

Table III lists orbital energies and electron occupancies of the electron donor in a water dimer at three temperatures, 0 K, 15 000 K, and 25 000 K. The purpose of the table is to illustrate the Fermi-Dirac distribution achieved by the coupled open systems that have partially equilibrated their number of electrons in the quasithermodynamic model of the dimer. By Eq. (22), these temperatures correspond to coupling strengths τ_{α} of 0.00 eV, 1.20 eV, and 2.00 eV, respectively, with the value of weight function g_{α} in Eq. (22) being 0.93. As the coupling strength increases, the orbital energies are lowered, and occupancies of the virtual orbitals increase. On average, for 38 occupied and virtual orbitals in the dimer, the orbital energy lowering is 0.03 eV for $\theta = 15\,000$ K and 0.32 eV for $\theta = 25\,000$ K; this large orbital energy shift is especially important for the HOMO and LUMO. One of the reasons that the orbital energies are lowered is the shielding effect, that is, as the temperature increases, the electron momentum increases, allowing occupancy of the higher energy orbitals. As a consequence, the electron densities in the inner shell become smaller, and the net interaction with inner orbitals and the nucleus becomes more attractive. The other reason is the complementary relationship between kinetic energy and potential energy due to the virial theorem.

The electrons distribute in a broader range of orbitals at the higher temperature due to the Fermi-Dirac distribution. To understand this better, we tested using a Gaussian-type distribution instead of the Fermi-Dirac distribution. When we did this, even higher temperature parameters were required to obtain the same amount of charge transfer as that obtained with the Fermi-Dirac distribution. This result indicates that the occupation of the high energy orbitals is an essential condition for the charge transfer states.

Because the amount of charge transferred and the charge transfer energy are physical observables and depend on the definition used, we focus first on the binding energy, which

TABLE III. Orbital energies [eV] and occupancies at 0 K, 15 000 K, and 25 000 K for the electron donor of water dimer calculated with GC-X-Pol with M06-2X/6-31G(d).

	$\theta = 0$		$\theta = 15\,000$		$\theta = 25\,000$	
	ϵ_i	f_i	ϵ_i	f_i	ϵ_i	f_i
1	-533.14	1.0	-533.27	1.000 000 000 0	-533.99	1.000 000 000 0
2	-29.51	1.0	-29.62	0.999 999 999 7	-30.22	0.999 998 425 9
3	-15.37	1.0	-15.47	0.999 958 717 9	-16.01	0.998 084 891 7
4	-11.42	1.0	-11.53	0.998 892 567 6	-12.05	0.986 315 204 0
5 (HOMO)	-9.44	1.0	-9.51	0.994 070 052 8	-9.89	0.960 705 034 3
6 (LUMO)	4.19	0.0	4.15	0.001 920 634 8	3.76	0.025 489 804 2
7	6.97	0.0	6.92	0.000 187 785 5	6.60	0.006 314 469 6
8	23.98	0.0	23.90	0.000 000 000 1	23.50	0.000 001 363 6
9	26.52	0.0	26.43	0.000 000 000 0	25.99	0.000 000 391 7
10	27.00	0.0	26.91	0.000 000 000 0	26.41	0.000 000 317 9
11	27.21	0.0	27.12	0.000 000 000 0	26.59	0.000 000 290 8
12	32.17	0.0	32.08	0.000 000 000 0	31.59	0.000 000 023 8
13	34.68	0.0	34.60	0.000 000 000 0	34.16	0.000 000 006 6
14	49.58	0.0	49.47	0.000 000 000 0	48.88	0.000 000 000 0

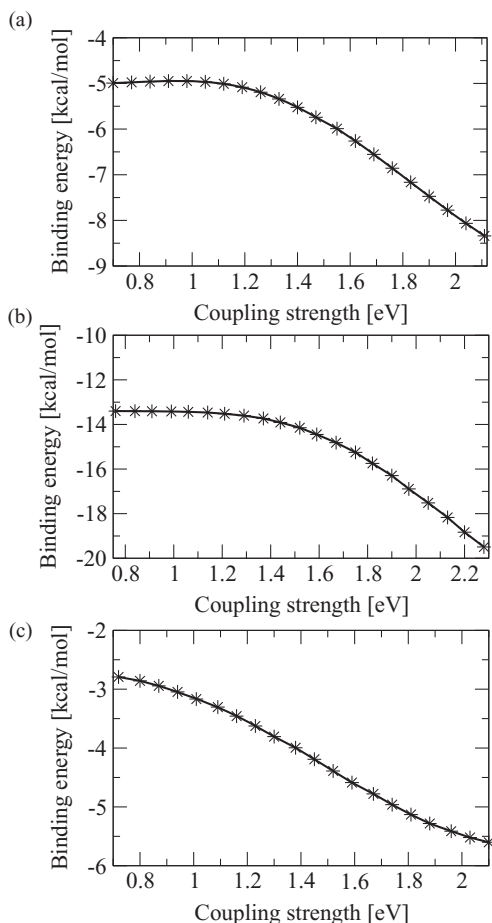


FIG. 4. Relationship between binding energy and coupling strength in (a) $\text{CH}_3\text{OH} \cdots \text{H}_2\text{O}$, (b) $\text{NH}_4^+ \cdots \text{H}_2\text{O}$, and (c) $\text{ClF} \cdots \text{H}_2\text{O}$.

is an observable. Figure 4 gives the relationship between the binding energy and the coupling strengths. As the coupling strength increases, the binding energy changes almost monotonically. However, the ratio of increase of binding energy is not linear, and it depends on the system, because of the dependence on the whole set of orbital energies. Figure 5 shows the coupling strength dependence of the charge separation. As can be expected, the amount of charge transfer becomes large as the coupling strength increases. The monotonic increase of charge separation with the coupling strength correlates with the binding energy stabilization for $\text{CH}_3\text{OH} \cdots \text{H}_2\text{O}$ and $\text{NH}_4^+ \cdots \text{H}_2\text{O}$. However, for $\text{ClF} \cdots \text{H}_2\text{O}$, the behavior of the charge separation is not monotonic; for example, the charge separation at coupling strength 1.52 eV ($\theta = 21\,000$ K) and 2.17 eV ($\theta = 30\,000$ K) is almost the same with the value being 0.011 e. This is because the intramolecular charge redistribution rather than the intermolecule charge redistribution is dominant at 30 000 K. The charge on the O atom is -0.81 e and -0.75 e for coupling strengths of 1.52 eV and 2.17 eV, respectively.

Figure 6 displays the energy difference between the HOMO of the electron donor and the LUMO of the electron acceptor and the HOMO of the electron acceptor and the LUMO of the electron donor. For hydrogen bonded systems in the both neutral–neutral and ion–neutral pairs, the en-

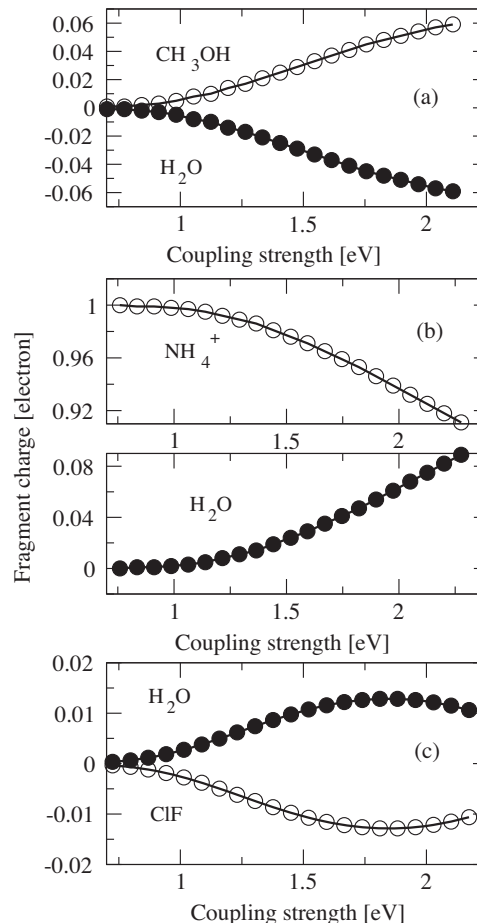


FIG. 5. Relationship between charge separation and coupling strength in (a) $\text{CH}_3\text{OH} \cdots \text{H}_2\text{O}$, (b) $\text{NH}_4^+ \cdots \text{H}_2\text{O}$, and (c) $\text{ClF} \cdots \text{H}_2\text{O}$. The charge of electron donor is plotted with closed circle and the charge of electron acceptor is plotted with open circle.

ergy gap between the HOMO of the electron donor and the LUMO of the electron acceptor increases, and the energy gap between the HOMO of the electron acceptor and the LUMO of the electron donor decreases. Thus, one energy gap increases, and another energy gap decreases. This indicates that the charge transfer from the HOMO of the electron acceptor to the LUMO of the electron donor also contributes to the system stabilization. For charge transfer systems, both of the energy gaps decrease. This behavior is reasonable for charge transfer systems, and this trend is observed for all four charge transfer systems.

V.B. Properties at bimolecular complexes

Figure 7 shows the RMS deviation of the charge transfer energy of GC-X-Pol from that estimated by the BLW-ED method, and this figure shows that $\theta = 25\,000$ K (the corresponding coupling strength differs for each system due to the difference of the weight g_α) provides the lowest RMS deviation with the value being 1.22 kcal/mol.

Table IV lists the calculated charge transfer energies in comparison with those calculated by the BLW method for the optimized coupling strength. The charge transfer energy is overestimated for the neutral–neutral pairs except for

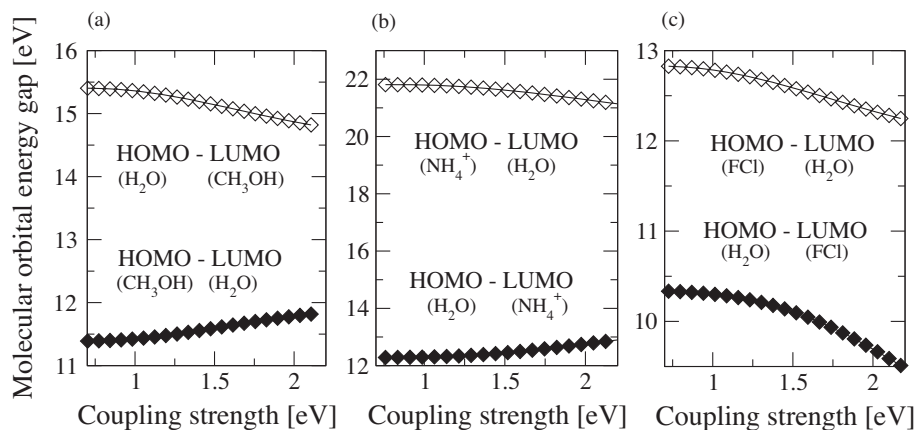


FIG. 6. Relationship between molecular orbital energy gap and coupling strength in (a) $\text{CH}_3\text{OH} \cdots \text{H}_2\text{O}$, (b) $\text{NH}_4^+ \cdots \text{H}_2\text{O}$, and (c) $\text{ClF} \cdots \text{H}_2\text{O}$. The two energy gaps correspond to the difference between the HOMO of the electron donor and the LUMO of the electron acceptor (closed diamond) and the difference between the HOMO of the electron acceptor and the LUMO of the electron donor (open diamond), respectively.

$\text{C}_2\text{H}_4 \cdots \text{ClF}$; on the other hand, it is underestimated for bimolecular complexes consisting of ion and neutral molecule. As mentioned in Sec. IV, the electrostatic, exchange repulsion, and polarization interactions are described using localized wave functions for both the X-Pol and BLW methods, and a major difference between these methods is the description of the intermolecular interactions—which employs a fully antisymmetrized wave function in one case and approximates the exchange repulsion empirically in the other. A second contribution is that parameters are only partially optimized in the present study. In the present initial test of the new method, we used constant values for the Δ , ζ in the GC-X-Pol method; therefore, further refinement is possible by changing these parameters so as to depend on the type of atom.

Figure 8 shows a cut through the binding energy surface of two of the hydrogen bonded systems and one charge transfer system. The inclusion of charge transfer enhances the binding energy relative to those obtained without charge transfer contributions. The contribution of the charge transfer is reduced as the two fragments become separated, indicating that the weight function g_α works correctly and that the parameter ζ is reasonable. By including the charge transfer ef-

fect, the distance corresponding to the minimum energy does not change appreciably; however, the binding energy profile is generated using the geometries optimized by full QM calculation, and there is possibility that the energy would change slightly if the angle were relaxed by the GC-X-Pol potential or if geometries were optimized using an X-Pol calculation with parameters to best reproduce the accurate results. In the short distance region, the binding energy profile deviates considerably from the full QM calculation, and this trend is observed for all energy profiles of the dimers calculated by both 0 K X-Pol and GC-X-Pol. The dominant reason for this is the form of the LJ potential function, that is, the R^{-12} term in LJ potential yields repulsive walls that are too steep because the Lennard-Jones parameters were not optimized for the M06-2X density functional. The exponential form is more realistic and may yield improved results. Furthermore, the representation of the electrostatic interaction by point charges from Mulliken population analysis is not accurate enough for quantitative construction of the quantum mechanical force field.^{6,84} It has been shown that the electrostatic interaction can be improved by including the charge penetration effect.^{84,85} This effect originates from the reduction of shielding by the electron cloud at shorter distances, and it would be interesting to test whether including charge penetration would improve the

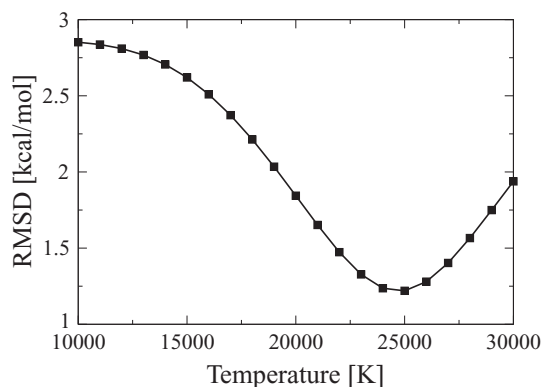


FIG. 7. Temperature dependence of RMS deviation of charge transfer energy estimated by GC-X-Pol method. The reference charge transfer energy is obtained by the BLW energy decomposition analysis for ten dimer systems (see Figure 3).

TABLE IV. Charge transfer energy [kcal/mol] calculated by GC-X-Pol with M06-2X/6-31G(d) at temperature 25 000 K with comparison of that of BLW with M06-2X/6-31+G(d, p).

	GC-X-Pol	BLW
(a) $\text{H}_2\text{O} \cdots \text{H}_2\text{O}$	-2.418	-0.916
(b) $\text{CH}_3\text{OH} \cdots \text{H}_2\text{O}$	-1.841	-1.019
(c) $\text{CH}_3\text{NH}_2 \cdots \text{H}_2\text{O}$	-0.852	-0.498
(d) $\text{CH}_3\text{NH}_3^+ \cdots \text{H}_2\text{O}$	-3.765	-4.348
(e) $\text{CH}_3\text{CO}_2^- \cdots \text{H}_2\text{O}$	-3.903	-4.993
(f) $\text{NH}_4^+ \cdots \text{H}_2\text{O}$	-2.897	-4.938
(g) $\text{ClF} \cdots \text{NH}_3$	-4.371	-2.801
(h) $\text{Cl}_2 \cdots \text{NH}_3$	-3.052	-1.428
(i) $\text{ClF} \cdots \text{H}_2\text{O}$	-2.447	-1.487
(j) $\text{ClF} \cdots \text{C}_2\text{H}_4$	-0.315	-0.631

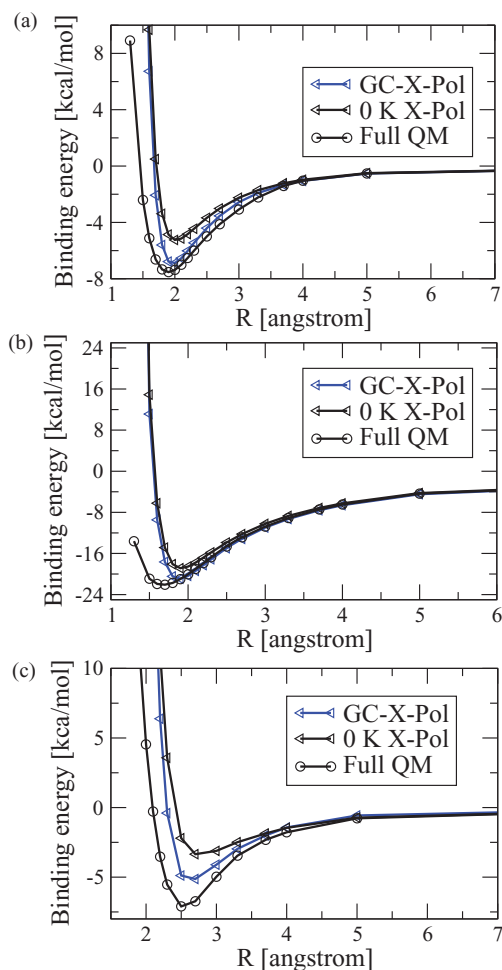


FIG. 8. Binding energy profile calculated by GC-X-Pol with M06-2X/6-31G(d), 0 K X-Pol with M06-2X/6-31G(d), and full QM calculation with M06-2X/6-31+G(d, p) for (a) $\text{CH}_3\text{OH} \cdots \text{H}_2\text{O}$, (b) $\text{NH}_4^+ \cdots \text{H}_2\text{O}$, and (c) $\text{ClF} \cdots \text{H}_2\text{O}$.

results obtained with X-Pol or GC-X-Pol. Nevertheless, it has been shown that with a single set of optimized Lennard-Jones parameters, the binding energies for a range of bimolecular complexes from the X-Pol method using a given DFT method can be fitted to yield an excellent agreement with values ob-

tained from full coupled cluster singlet and double excitation (CCSD(T)) optimizations.³²

Although Mulliken population analysis can lead to unphysical results when applied uncritically or with large basis sets, here it provides a useful measure of the amount of charge transfer between fragments; for small interfragment separation, it is useful because we use a small basis set without diffuse function, and for interfragment separation it is justifiable because the overlaps of orbitals on different fragments becomes very small. Table V summarizes the charge separation calculated by Mulliken population analysis for the ten dimer systems at their equilibrium distances. We can see that in all ten cases GC-X-Pol provides a direction of the charge transfer that is consistent with that obtained by Mulliken population analysis of the full QM calculation. Here, as already specified in Subsection III A, we used the 6-31G(d) basis set for the X-Pol calculation because 6-31G(d) basis sets provide the reasonable atomic charge and polarization in the X-Pol method. We used the 6-31+G(d, p) basis set for the full QM calculation because it provides more accurate reference data. We believe that the comparison of the amount of charge transfer with that of full QM calculation is a less definitive measures of success than the energy stabilization because charges are not observable quantities, and no rigorous definition of the atomic charge exists; moreover, atomic charge largely depends to a greater extent on the employed level of theory and basis set.⁸⁶

The electronegativity of each fragment is equal for the water dimer system, and the local difference of the electronegativity before equalization is a trigger of the charge transfer in this system. In the linear form of water dimer (see Fig. 3(a)), the electronegativity of oxygen is larger than that of hydrogen, and the charge flows from the water of the proton donor to the water of the electron acceptor. According to the atomic polar tensor analysis used by Åstrand *et al.*,⁸⁷ the electron moves from the proton donor to the acceptor, which is consistent with the present direction of charge transfer. The net effect of intermolecular charge transfer, which is of quantum mechanical origin, is reflected by increased atomic charges that enhance Coulomb interactions between the donor and acceptor molecules. It is noteworthy that intramolecular charge

TABLE V. Charge separation [electron] calculated by GC-X-Pol with M06-2X/6-31G(d) and full QM calculation with M06-2X/6-31G+(d, p). The charge separation in 0 K X-Pol is listed as a reference.

	GC-X-Pol		0 K X-Pol		Full QM	
	ED	EA	ED	EA	ED	EA
(a) $\text{H}_2\text{O}(\text{ED}^a) \cdots \text{H}_2\text{O}(\text{EA}^b)$	0.046	-0.046	0.0	0.0	0.012	-0.012
(b) $\text{CH}_3\text{OH}(\text{ED}) \cdots \text{H}_2\text{O}(\text{EA})$	0.044	-0.044	0.0	0.0	0.013	-0.013
(c) $\text{CH}_3\text{NH}_2(\text{ED}) \cdots \text{H}_2\text{O}(\text{EA})$	0.040	-0.040	0.0	0.0	0.012	-0.012
(d) $\text{CH}_3\text{NH}_3^+(\text{EA}) \cdots \text{H}_2\text{O}(\text{ED})$	0.020	0.980	0.0	1.0	0.050	0.950
(e) $\text{CH}_3\text{CO}_2^-(\text{ED}) \cdots \text{H}_2\text{O}(\text{EA})$	-0.972	-0.028	-1.0	0.0	-0.952	-0.048
(f) $\text{NH}_4^+(\text{EA}) \cdots \text{H}_2\text{O}(\text{ED})$	0.054	0.946	0.0	1.0	0.040	0.960
(g) $\text{ClF}(\text{EA}) \cdots \text{NH}_3(\text{ED})$	0.028	-0.028	0.0	0.0	0.069	-0.069
(h) $\text{Cl}_2(\text{EA}) \cdots \text{NH}_3(\text{ED})$	0.069	-0.069	0.0	0.0	0.042	-0.042
(i) $\text{ClF}(\text{EA}) \cdots \text{H}_2\text{O}(\text{ED})$	0.012	-0.012	0.0	0.0	0.027	-0.027
(j) $\text{C}_2\text{H}_4(\text{ED}) \cdots \text{ClF}(\text{EA})$	0.041	-0.041	0.0	0.0	0.044	-0.044

^aED: electron donor.

^bEA: electron acceptor.

TABLE VI. Molecular orbital energies [eV] around frontier orbitals before(0 K X-Pol) and after(GC-X-Pol) charge transfer.

	CH ₃ OH...H ₂ O				NH ₄ ⁺ ...H ₂ O				ClF...H ₂ O			
	0 K X-Pol		GC-X-Pol		0 K X-Pol		GC-X-Pol		0 X-Pol		GC-X-Pol	
	CHCH ₃ OH ED	H ₂ O EA	CH ₃ OH ED	H ₂ O EA	NH ₄ ⁺ EA	H ₂ O ED	NH ₄ ⁺ EA	H ₂ O ED	ClF EA	H ₂ O ED	ClF EA	H ₂ O ED
HOMO-2	-12.76	-16.81	-13.12	-16.69	-23.45	-21.51	-23.28	-22.05	-14.91	-16.85	-14.71	-17.10
HOMO-1	-10.19	-12.99	-10.55	-12.92	-23.44	-18.37	-23.28	-18.86	-10.15	-12.92	-9.91	-13.17
HOMO	-8.59	-10.89	-8.86	-10.73	-23.12	-15.68	-23.01	-16.03	-10.14	-10.88	-9.90	-11.02
LUMO	4.51	2.79	4.25	2.83	-3.39	-1.31	-3.34	-1.65	-0.54	2.68	-1.15	2.51
LUMO+1	5.66	5.16	5.42	5.28	-1.37	1.08	-1.25	0.75	10.47	5.06	10.43	4.93
LUMO+2	6.38	22.57	6.16	22.70	-1.36	17.78	-1.24	17.40	13.23	22.52	13.17	22.35

redistribution accompanies the charge transfer, for example, the site charge on the oxygen atom in the electron acceptor is $q_O = -0.803$ e as compared to the corresponding reference charge of $q_O = -0.755$ e; this charge redistribution $\Delta q_O = 0.048$ e is as great as the interfragment charge separation, 0.046 e. This result indicates that one should not consider charge transfer separately from electronic polarization.

As can be seen from Eq. (21), the Fermi–Dirac distribution of electron density is determined by the configuration of molecular orbitals at constant coupling strength and chemical potential. Table VI shows the orbital energies around the frontier orbitals. We can see that the HOMO and LUMO that give the lowest energy gap between the electron donor and the electron acceptor are located on the electron donor and the electron acceptor, respectively, both before (0 K X-Pol) and after (GC-X-Pol) charge transfer. This is the dominant reason that the direction of charge transfer is described correctly by GC-X-Pol.

VI. CONCLUDING REMARKS

In this work, we proposed a grand canonical X-Pol method to describe charge transfer in the X-Pol potential. In this method, the electrons are described by the Fermi–Dirac distribution. To express dependence of charge transfer on the fragment separation correctly, we devised a physically motivated form of the chemical potential, and we re-interpreted the temperature in the distribution function as a coupling strength.

In the GC-X-Pol method, the charge transfer state and the reference state are characterized by electronic occupation of virtual orbitals, and it is observed that the electrons distribute in a broad range of orbitals due to the Fermi–Dirac distribution. It was found that intramolecular charge redistribution is promoted as well as intermolecular redistribution. The key validations are that the stabilization energy by charge transfer is comparable with the charge transfer (delocalization) energy calculated by the BLW method, and the calculated charge separations are close to the values derived by the Mulliken population analysis of full QM calculations.

Further refinement is possible for this method. One possible refinement is further optimization of the parameters in the weight function g_α , namely Δ and ζ . In the present study, we set the values of these parameters to pre-determined constants, but allowing them to depend on the type of atom should make the GC-X-Pol method a more quantitative model. The

other possible refinement is further parametrization of the temperature-like parameter θ . In the present study, θ is roughly determined for a small number of systems. In future work, we should parametrize it for a larger number of systems. In the ten dimer systems, it is found that the charge transfer energy is overestimated for the neutral–neutral systems except for C₂H₄...ClF, and underestimated for the ion–neutral systems. If such a general trend is revealed by applying the method to more systems, the temperature parameter θ can be determined for each system according to its bond type and charge state to obtain a more accurate charge transfer model.

Although the method has been presented in the context of X-Pol, many elements of the method are more general, and the same strategy could be used to include charge transfer into other fragment methods. This would solve a long-standing problem by which charge transfer is treated at a lower level than charge polarization in molecular modeling.

ACKNOWLEDGMENTS

The authors are grateful to Hannah Leverentz for assistance with the calculations. This work is supported by the NIH (Grant No. NIGMS/1RC1GM091445) and NSF (Grant No. CHE09-56776).

- ¹R. S. Mulliken, *J. Am. Chem. Soc.* **72**, 600 (1950).
- ²W. B. Person, R. E. Humphrey, W. A. Deskin, and A. I. Popov, *J. Am. Chem. Soc.* **80**, 2047 (1958).
- ³H. Ratajczak and W. J. Orville-Thomas, *J. Mol. Struct.* **14**, 155 (1972)
- ⁴M. S. A. Abdou, F. P. Orfino, Y. Son, and S. Holdcroft, *J. Am. Chem. Soc.* **119**, 4518 (1997).
- ⁵Y. Zhang and X.-Z. You, *J. Comput. Chem.* **22**, 327 (2001).
- ⁶A. Karpfen, *Theor. Chem. Acc.* **110**, 1 (2003).
- ⁷K. Kitaura and K. Morokuma, *Int. J. Quantum Chem.* **10**, 325 (1976).
- ⁸W. J. Stevens and W. H. Fink, *Chem. Phys. Lett.* **139**, 15 (1987).
- ⁹E. D. Glendening and A. Streitwieser, *J. Chem. Phys.* **100**, 2900 (1994).
- ¹⁰Y. Mo, J. Gao, and S. D. Peyerimhoff, *J. Chem. Phys.* **112**, 5530 (2000).
- ¹¹W. A. Lathan and K. Morokuma, *J. Am. Chem. Soc.* **97**, 6624 (1975).
- ¹²G. Nadig, L. C. Van Zant, S. L. Dixon, and K. M. Merz, *J. Am. Chem. Soc.* **120**, 5593 (1998).
- ¹³A. van der Vaart and K. M. Merz, Jr., *J. Am. Chem. Soc.* **121**, 9182 (1999).
- ¹⁴A. van der Vaart and K. M. Merz, *J. Chem. Phys.* **116**, 7380 (2002).
- ¹⁵Y. Mo and J. Gao, *J. Phys. Chem. B* **110**, 2976 (2006).
- ¹⁶J. Gao, D. Habibollazadeh, and L. Shao, *J. Phys. Chem.* **99**, 16460 (1995).
- ¹⁷A. Morita and S. Kato, *J. Chem. Phys.* **108**, 6809 (1998).
- ¹⁸T. A. Halgren and W. Damm, *Curr. Opin. Struct. Biol.* **11**, 236 (2001).
- ¹⁹P. Ren and J. W. Ponder, *J. Comput. Chem.* **23**, 1497 (2002).
- ²⁰G. A. Kaminski, H. A. Stern, B. J. Berne, R. A. Friesner, Y. X. Cao, R. B. Murphy, R. Zhou, and T. A. Halgren, *J. Comput. Chem.* **23**, 1515 (2002).

- ²¹A. D. J. MacKerell, *J. Comput. Chem.* **25**, 1584 (2004).
- ²²S. Patel, A. D. Mackerell, Jr., and C. L. Brooks III, *J. Comput. Chem.* **25**, 1504 (2004).
- ²³V. M. Anisimov, G. Lamoureux, I. V. Vorobyov, N. Huang, B. Roux, and A. D. MacKerell, Jr., *J. Chem. Theory Comput.* **1**, 153 (2005).
- ²⁴E. Harder, V. M. Anisimov, I. V. Vorobyov, P. E. M. Lopes, S. Y. Noskov, A. D. MacKerell, Jr., and B. Roux, *J. Chem. Theory Comput.* **2**, 1587 (2006).
- ²⁵W. L. Jorgensen, *J. Chem. Theory Comput.* **3**, 1877 (2007).
- ²⁶W. Xie, J. Pu, A. D. Mackerell, Jr., and J. Gao, *J. Chem. Theory Comput.* **3**, 1878 (2007).
- ²⁷M. Isegawa and S. Kato, *J. Chem. Theory Comput.* **5**, 2809 (2009).
- ²⁸J. W. Ponder, C. Wu, P. Ren, V. S. Pande, J. D. Chodera, M. J. Schnieders, I. Haque, D. L. Mobley, D. S. Lambrecht, R. A. DiStasio, Jr., M. Head-Gordon, G. N. I. Clark, M. E. Johnson, and T. Head-Gordon, *J. Phys. Chem. B* **114**, 2549 (2010).
- ²⁹J. Gao, *J. Phys. Chem. B* **101**, 657 (1997).
- ³⁰W. Xie and J. Gao, *J. Chem. Theory Comput.* **3**, 1890 (2007).
- ³¹W. Xie, L. Song, D. G. Truhlar, and J. Gao, *J. Chem. Phys.* **128**, 234108 (2008).
- ³²L. Song, J. Han, Y. Lin, W. Xie, and J. Gao, *J. Phys. Chem. A* **113**, 11656 (2009).
- ³³H. Leverentz, J. Gao, and D. G. Truhlar, *Theor. Chem. Acc.* **129**, 3 (2011).
- ³⁴A. Cembran, P. Bao, Y. Wang, L. Song, D. G. Truhlar, and J. Gao, *J. Chem. Theory Comput.* **6**, 2469 (2010).
- ³⁵H. Li, M. S. Gordon, and J. H. Jensen, *J. Chem. Phys.* **124**, 214108 (2006).
- ³⁶P. N. Day, J. H. Jensen, M. S. Gordon, S. P. Webb, W. J. Stevens, M. Kraus, D. Garmer, H. Basch, and D. Cohen, *J. Chem. Phys.* **105**, 1968 (1996).
- ³⁷M. S. Gordon, M. A. Freitag, P. Bandyopadhyay, J. H. Jensen, V. Kairys, and W. J. Stevens, *J. Phys. Chem. A* **105**, 293 (2001).
- ³⁸A. J. Stone, *Chem. Phys. Lett.* **211**, 101 (1993).
- ³⁹N. D. Mermin, *Phys. Rev.* **137**, 1441 (1965).
- ⁴⁰D. A. McQuarrie, *Statistical Mechanics* (Harper Collins, New York, 1976).
- ⁴¹P. Hohenberg and W. Kohn, *Phys. Rev.* **136**, 864 (1964).
- ⁴²K. Shiratori and K. Nobusada, *J. Chem. Phys. Lett.* **451**, 158 (2008).
- ⁴³T. Biben and D. Frenkel, *J. Phys.: Condens. Matter* **14**, 9077 (2002).
- ⁴⁴M. P. Grumbach, Detlef Hohl, R. M. Martint, and R. Car, *J. Phys.: Condens. Matter* **6**, 1999 (1994).
- ⁴⁵M. Weinert and J. W. Davenport, *Phys. Rev. B* **45**, 13709 (1992).
- ⁴⁶R. M. Wentzcovitch, J. L. Martins, and P. B. Allen, *Phys. Rev. B* **45**, 11372 (1992).
- ⁴⁷R. T. Sanderson, *Science* **114**, 670 (1951).
- ⁴⁸R. G. Parr, R. A. Donnelly, M. Levy, and W. E. Palke, *J. Phys. Chem.* **68**, 3801 (1978).
- ⁴⁹W. Kohn, A. D. Becke, and R. G. Parr, *J. Phys. Chem.* **100**, 12974 (1996).
- ⁵⁰W. J. Mortier, S. K. Ghosh, and S. Shankar, *J. Am. Chem. Soc.* **108**, 4315 (1986).
- ⁵¹S. W. Rick, S. J. Stuart, and B. J. Berne, *J. Chem. Phys.* **101**, 6141 (1994).
- ⁵²A. K. Rappe and W. A. Goddard, III, *J. Phys. Chem.* **95**, 3358 (1994).
- ⁵³D. M. York and W. Yang, *J. Chem. Phys.* **104**, 159 (1996).
- ⁵⁴H. A. Stern, G. A. Kaminski, J. L. Banks, R. Zhou, B. J. Berne, and R. A. Friesner, *J. Phys. Chem. B* **103**, 4730 (1999).
- ⁵⁵R. Chelli and P. Procacci, *J. Chem. Phys.* **117**, 9175 (2002).
- ⁵⁶P. Bultinck, W. Langenaeker, P. Lahorte, F. De Proft, P. Geerlings, C. Van Alsenoy, and J. P. Tollenaere, *J. Phys. Chem. A* **106**, 7887 (2002).
- ⁵⁷P. Bultinck, W. Langenaeker, P. Lahorte, F. De Proft, P. Geerlings, C. Van Alsenoy, and J. P. Tollenaere, *J. Phys. Chem. A* **106**, 7895 (2002).
- ⁵⁸J. Gasteiger and M. Marsili, *Tetrahedron* **36**, 3219 (1980).
- ⁵⁹R. Chelli, P. Procacci, R. Righini, and S. Califano, *J. Chem. Phys.* **111**, 8569 (1999).
- ⁶⁰J. Morales and T. J. Martinez, *J. Phys. Chem. A* **105**, 2842 (2001).
- ⁶¹J. Chen and T. J. Martinez, *Chem. Phys. Lett.* **438**, 315 (2007).
- ⁶²D. Mathieu, *J. Chem. Phys.* **127**, 224103 (2007).
- ⁶³G. L. Warren, J. E. Davis, and S. Patel, *J. Chem. Phys.* **128**, 144110 (2008).
- ⁶⁴J. E. Davis, G. L. Warren, and S. Patel, *J. Phys. Chem. B* **112**, 8298 (2008).
- ⁶⁵H. S. Smalø, P.-O. Åstrand, and L. Jensen, *J. Chem. Phys.* **131**, 044101 (2009).
- ⁶⁶K. Aoki, S. Tanaka, and T. Nakano, *Chem-Bio Informatics* **9**, 30 (2009).
- ⁶⁷H. Nakano, T. Yamamoto, and S. Kato, *J. Chem. Phys.* **132**, 044106 (2010).
- ⁶⁸H. P. Pritchard, *J. Am. Chem. Soc.* **85**, 1876 (1963).
- ⁶⁹P. D. Lyne, M. Hodoscek, and M. Karplus, *J. Phys. Chem. A* **103**, 3462 (1999).
- ⁷⁰R. S. Mulliken, *J. Chem. Phys.* **23**, 1833 (1955).
- ⁷¹T. A. Koopmans, *Physica* **1**, 104 (1933).
- ⁷²Y. Zhao and D. G. Truhlar, *Theor. Chem. Acc.* **120**, 215 (2008).
- ⁷³W. J. Hehre, L. Radom, P. v. R. Schleyer, and J. A. Pople, *Ab initio Molecular Orbital Theory* (Wiley, New York, 1986).
- ⁷⁴M. Gussoni, M. N. Ramos, C. Castiglioni, and G. Zerbi, *Chem. Phys. Lett.* **142**, 515 (1987).
- ⁷⁵J. Li, T. Zhu, C. J. Cramer, and D. G. Truhlar, *J. Phys. Chem. A* **102**, 1820 (1998).
- ⁷⁶P. Zhang, P. Bao, and J. Gao, *Comput. Chem.* **32**, 2127 (2011).
- ⁷⁷J. Gao, *ACS Symp. Ser.* **569**, 8 (1994).
- ⁷⁸D. Riccardi, G. Li, and Q. Cui, *J. Phys. Chem. B* **108**, 6467 (2004).
- ⁷⁹J. Wang, R. M. Wolf, J. W. Caldwell, P. A. Kollman, and D. A. Case, *J. Comp. Chem.* **25**, 1157 (2004).
- ⁸⁰A. Bondi, *J. Phys. Chem.* **68**, 441 (1964).
- ⁸¹E. Ruiz, D. R. Salahub, and A. Vela, *J. Phys. Chem.* **100**, 12265 (1996).
- ⁸²I. Alkorta, I. Rozas, and J. Elguero, *J. Phys. Chem. A* **102**, 9278 (1998).
- ⁸³Y. Zhao and D. G. Truhlar, *J. Chem. Theory Comput.* **1**, 415 (2005).
- ⁸⁴B. Wang and D. G. Truhlar, *J. Chem. Theory Comput.* **6**, 3330 (2010).
- ⁸⁵M. A. Freitag, M. S. Gordon, J. H. Jensen, and W. J. Stevens, *J. Chem. Phys.* **112**, 7300 (2000).
- ⁸⁶J. Cioslowski, *J. Am. Chem. Soc.* **111**, 8333 (1989).
- ⁸⁷P.-O. Åstrand, K. Ruud, K. V. Mikkelsen, and T. Helgaker, *J. Phys. Chem. A* **102**, 7686 (1998).